On the cusp of x-ray tomographic mapping of the human brain and its 10^{11} cells

Bert Müller*[a,b]
[a]Biomaterials Science Center, Department of Biomedical Engineering, University of Basel, 4123 Allschwil, Switzerland; [b]Biomaterials Science Center, Department of Clinical Research, University Hospital Basel, 4031 Basel, Switzerland

ABSTRACT

The human brain contains 86 billion cells, but so far only a part could be visualized. The task corresponds to the acquisition and treatment of a petabyte-size dataset – analogous to plotting every star in the Milky Way. We demonstrated the feasibility of cellular-resolution full-brain imaging for ethanol-immersed and paraffin-embedded human brain using the tomography setup at the beamline P07 (PETRA III, DESY, Hamburg, Germany), which is operated by the Helmholtz-Zentrum Hereon. Because the beam size and the number of detector pixels limit the field-of-view to 6 mm, we decided to stitch these radiographs to projections 90,000 pixels wide. The reconstructed slices allow for the detection of cells, although they contain severe artefacts. The next challenge is the optimization of the data acquisition, so that an entire brain can be made visible using typical beamtime applications. Reconstruction, artefact removal, and dissemination of such a human brain atlas is a task we are faced to. It will create a paradigm for investigating other human organs, high-performance engineering devices, and unique cultural heritage objects related to data of terabyte or even petabyte size.

Keywords: Computed tomography, microtomography, synchrotron radiation, radiograph stitching, murine and human brain, dissemination of big data, human brain embedding, ethanol-immersed tissue.

1. INTRODUCTION

The human brain coordinates essential human abilities such as memory, vision, respiration, and body temperature regulation. Its diameter is on the order of 10 cm. The brain's cells are on the order of micrometers, the synaptic connections can be thinner than 100 nm, and the morphological changes on the order of a few nanometers can affect brain circuit function. Thus, comprehensive brain mapping requires a multi-modal approach for imaging length scales across eight or more orders of magnitude in each dimension. Currently, the visualization of the anatomical features on the micrometer or even nanometer level is only obtained after physical sectioning that leads to preparation artefacts and, generally, a reduction of spatial resolution in at least one direction. Murine brains, 3,000 times smaller than those of humans, however, have been successfully visualized with isotropic sub-micrometer voxels by means of synchrotron radiation-based micro computed tomography [1]. This approach takes advantage of the penetration power of almost parallel, hard X rays to circumvent physical sectioning of tissue. We push the current limits of this imaging technique toward subcellular resolution of an entire human brain for basic science and future medical applications. For this purpose, we prepare human brains immersed in pure ethanol and embedded in paraffin advancing the established histology protocols. Currently, paraffin-embedded human brains contain numerous voids and cracks caused by the 10% shrinkage during paraffin solidification. These defects, to be circumvented, compromise phase tomography imaging using hard X rays. The radiographic projections of the human brain can be acquired and stitched at the tomography setup of the beamline P07, PETRA III, DESY, Hamburg, Germany, with an effective pixel size close to 1 µm. Very recently, we demonstrated feasibility for cross-sections of entire human brains immersed in ethanol and embedded in paraffin [2]. We developed software tools to reconstruct the big phase tomography data [2]. Note the data of a single slice have a size of nearly 20 GB, which gives rise to about 1,000 TB for the whole human brain to be stored and treated. This approach also includes removing ring artefacts arising from prominent features such as highly X-ray absorbing components and detector inhomogeneity.

*bert.mueller@unibas.ch; phone +41 61 207 5430; fax 41 61 207 5499; www.bmc.unibas.ch

Developments in X-Ray Tomography XV, edited by Bert Müller, Ge Wang,
Proc. of SPIE Vol. 13152, 1315202 · © 2024 SPIE
0277-786X · doi: 10.1117/12.3032298

It is planned to make the generated atlas of the entire human brain publicly available, starting with creating an efficient data processing and storage pipeline for the available 3.6 TB data of the human brain slice with isotropic 1.3 µm voxels [2]. The three-dimensional representation of the entire brain with true micrometer resolution will be non-rigidly registered to the EBRAINS' human brain atlases to allow usage of their atlas services. The registered image will be disseminated via EBRAINS after conversion to shared Neuroglancer format for efficient data handling. Such a comprehensive imaging dataset of the entire human brain will have impact for teaching purposes. The gained knowledge in brain preparation as well as acquisition and handling of such big imaging data should be applied to any human organ in health and disease so that related diagnosis and treatment planning will include microanatomical features on the level of individual cells. In future, the envisioned imaging should be applied to other unique objects, such as in materials and museum sciences.

2. NEUROIMAGING ACROSS LENGTH SCALES COVERING NINE ORDERS OF MAGNITUDE IN EACH DIMENSION

For conventional neuroimaging techniques, one finds a trade-off between imaged volume and spatial resolution [3]. High-resolution techniques, such as electron microscopy and histology, suffer from limited penetration depth thus require physical sectioning, while full brain clinical imaging with magnetic resonance imaging (MRI) and computed tomography (CT) can only reach sub-millimeter resolution. Figure 1 shows that virtual histology based on hard X-ray tomography can extend conventional histology for volumetric neuroimaging, potentially unlocking both high resolution and large imaged volume, though data sizes will soon reach the petabyte scale.

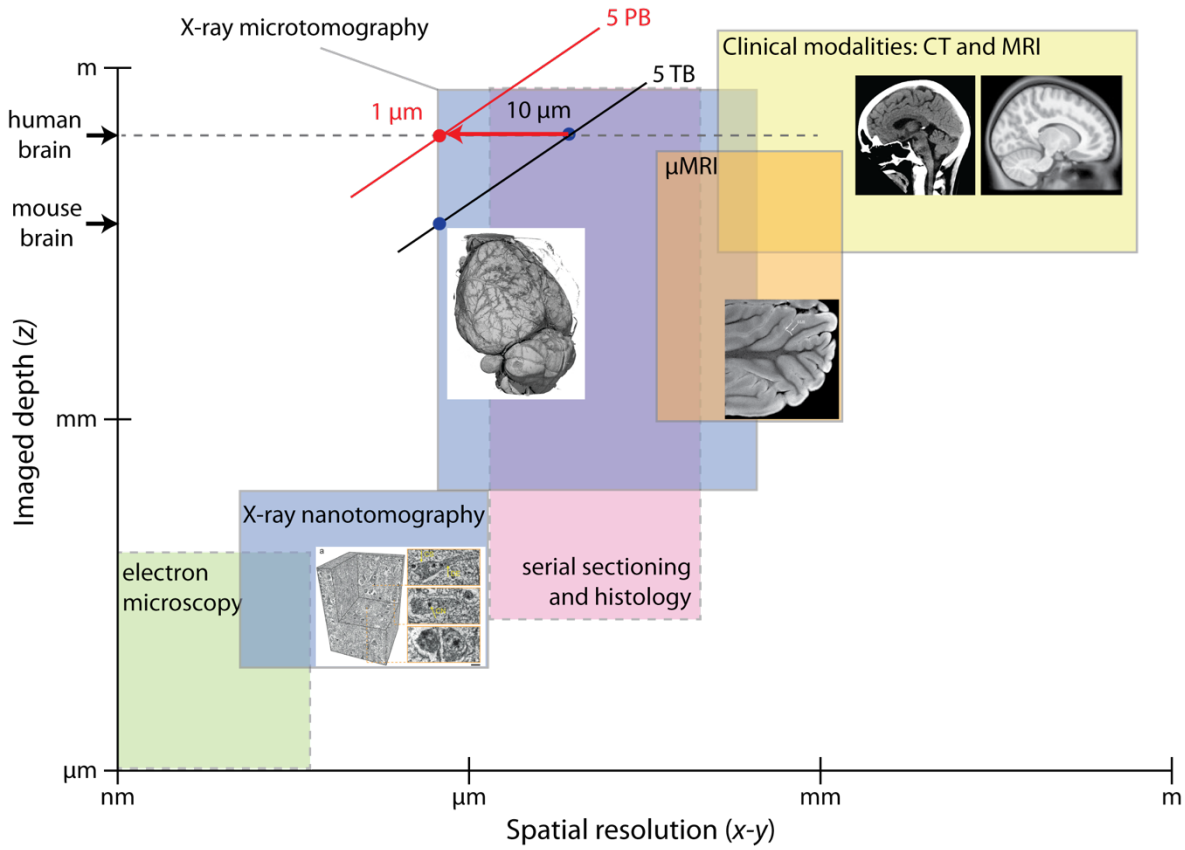

Figure 1. Neuroimaging of the entire human brain with cellular resolution is challenging because data of petabyte size must be recorded, reconstructed, and analyzed. The dissemination of the acquired information is also a challenge, because the specialists only need a small part of the available data, as we know from platforms as Google Earth.

3. MAGNETIC RESONANCE IMAGING OF THE BRAIN

For the *in vivo* visualization of the human brain on the macroscopic scale, magnetic resonance imaging (MRI) is the gold standard, as it provides excellent contrast and avoids ionizing radiation. This method is based on the relaxation of nuclear spins of hydrogen atoms. *In vivo* and *in situ* volumetric datasets can be obtained with voxel sizes down to a fraction of a millimeter [4]. Numerous acquisition sequences have been used to obtain appropriate contrast for clinical diagnostics [4] as well as related scientific studies. Specialized sequences for diffusion-weighted MRI, give access to microanatomical features including fiber trajectories or axon diameters [5]. Despite their voxel sizes hardly better than a cubic millimeter, MRI has been used as reference for aligning and correcting histological slices for preparing brain atlases, see, for example, the BigBrain project [6].

Specific scanners such as those employed for small animal imaging and human brain segments, can reach magnetic fields of 9 T and above. Imaging with these high-field-strength scanners is frequently termed magnetic resonance microscopy (µMRI) and can reach voxel lengths of several tens of micrometers [4]. For cubic centimeter-sized volumes, the acquisition time is on the order of ten hours. This method was applied on murine brains to understand and characterize the effects of genotype on anatomy, physiology, and behavior and, ultimately, the role of genotype in disease development [7]. It also served as imaging technique to establish a three-dimensional neuroanatomical atlas of the entire mouse brain [8]. Combining active MRI stains and optimized tissue preparation with µMRI can allow for correlating the volumetric data to a series of histology slides, giving insights onto the cytoarchitecture and cellular distribution of active stains [9]. Although the cytoarchitecture of a human cerebral cortex can be investigated with sub-100 µm voxel width [10] true cellular resolution is generally inaccessible. The current state of the art is characterized by recently published data of an *ex vivo* mouse brain with 20 µm voxels acquired with a scan time of 27 hours using a 15 T MRI scanner [11]. µMRI also permitted the identification of iron-laden oligodendrocytes in human cortical gray matter and cortical lesion segments [12]. Thus, such *ex vivo* studies allow for the visualization of the largest cells of the brain including the Purkinje cells.

4. CLASSICAL HISTOLOGY FOR BRAIN MAPPING

Histology is the gold standard for histopathological analysis and validation of neural tissue imaging. It has been employed for the identification of tissue, *e.g.* grey and white matter [13], for automated cell counting [14] and to map the brain's cytoarchitecture [15]. Currently available human brain reference atlases with cellular or nearly cellular resolution, such as the ALLEN Human Brain Reference Atlas [16] or the BigBrain model [6], consist of histological sections combined with non-invasive three-dimensional imaging. The ALLEN Human Brain Reference atlas, for instance, comprises three-dimensional MRI and diffusion-weighted imaging datasets, combined with histological slices with micrometer resolution.

The construction of three-dimensional data from two-dimensional histological sections is usually achieved by registration to a reference dataset such as from MRI. Several pipelines have been proposed, for instance registering MRI volumes and histological slices directly [17], or taking photographs of blocks during slicing to be used as an intermediate modality [18]. Distortions in the histological sections such as folds and tears pose challenges for registration, which have been addressed, *e.g.*, by introducing a probabilistic model for the deformations [19].

5. VIRTUAL HISTOLOGY AS A NEUROIMAGING TOOL

The visualization of the brain cytoarchitecture with X-ray microtomography (µCT) has conventionally relied on heavy-metal staining [20, 21]. Many stains have been suggested, such as osmium-based [22, 23], iodine-based [24, 25], and Golgi-Cox mercury-based impregnation [26, 27]. Unfortunately, selection and usage of X-ray contrast agents is sample- and target-specific, hence presenting a barrier for non-experts. Nevertheless, the first successful µCT cell imaging *post mortem* was also based on osmium staining [28].

Phase-contrast X-ray imaging offers higher density resolution than absorption contrast [29], allowing for imaging of the minute native density differences in brain tissue without staining [30, 31]. This has enabled label-free imaging of cyto- and angioarchitecture of whole rodent brains [32, 33]. It has also been used for the quantitative analysis of cytoarchitecture within neuronal volumes up to tens of cubic millimeters in size for mice and humans [34-36]. Such cellular-resolution neuroimaging has even been demonstrated with laboratory-based systems [36-38]. Unique possibilities such as capillary-

level visualization of amyloid-angiopathy were demonstrated in a mouse brain model of ALZHEIMER's disease [39]. Hard X-ray nano-tomography has also shown promise for neuroimaging, with isotropic spatial resolution down to and even below the optical limit [40, 41].

Thus, virtual histology based on hard X-ray µCT [42], also called three-dimensional X-ray histology, is an emerging neuroimaging technique that can reveal the brain's cellular structure in three dimensions [34-38] and complement MRI and conventional histology as part of a multi-modal imaging strategy [43, 44]. For example, in a study on ALZHEIMER's disease, a correlation of classical histology and X-ray phase-contrast tomography showed that some hallmarks of the disease, such as an accumulation of microglia, are directly visible with X-ray tomography, while others, such as senile plaques, can only be observed indirectly [37].

6. LARGE VOLUME BRAIN MAPPING WITH MICROTOMOGRAPHY

While hard X-ray penetration of soft tissues theoretically allows for µCT of entire centimeter-sized brains, the field-of-view (FOV) for micrometer resolution imaging is usually limited by detector array size. Standard detectors for X-ray µCT are based on CMOS cameras coupled to a scintillator via light microscope objectives, thus consisting of a few thousand pixels in each of the two directions. For spatial resolution of 1 µm, *i.e.* a pixel size below 0.5 µm, a single detector FOV provides tomographic reconstruction of only a few cubic millimeters. The volume of a mouse brain is about 500 mm^3 and that of a human brain is about 10^6 mm^3, therefore the FOV must be significantly extended for brain mapping applications.

Translation of the sample along the axis of rotation allows for extension of FOV via helical scans or, more commonly, stitched reconstructions from several height steps. Approaches for extending the FOV orthogonal to the rotation axis generally fall into three categories: (i) stitching reconstructions from a grid of local scans, hereafter denoted as reconstruction stitching, (ii) stitching projections taken with a common center-of-rotation, hereafter referred to as projection stitching, or (iii) a combination of the two, hereafter hybrid stitching [45-48]. Reconstruction stitching allows for standard reconstruction provided by most µCT beamline facilities, though corrections are needed for well-known local tomography artefacts from truncated sinograms [49-51]. For long measurements of dose-sensitive samples, dedicated correction of deformations with non-rigid stitching is beneficial [52, 53]. Projection stitching is more dose- and time-efficient [45], though it requires a higher precision in alignment of the rotation axis and a dedicated pipeline for mosaic stitching of projections and reconstruction of huge datasets [47, 48].

These mosaic-style acquisitions have been gaining traction in the virtual histology community. Microtomography of a mouse brain with 1.17 µm pixel size was used to validate fiber orientations in diffusion MRI [54]. Similar imaging was shown as a critical link from full-brain MRI to large-volume serial electron microscopy to visualize mouse brain structures covering five orders of magnitude in length [55]. For human brain imaging, hierarchical phase contrast imaging was demonstrated for large organs at the European Synchrotron Radiation Facility [56]. An entire human brain was imaged at 25 µm voxel size, with local tomography providing magnified views at 6 and 2.5 µm voxels [56]. Exploration, registration with existing atlases, e.g. the ALLEN Mouse Brain Common Coordinate Framework [57] or the BigBrain project for the human brain [6], and public availability remain challenges for such teravoxel datasets.

7. DISSEMINATION OF LARGE BRAIN VOLUME DATA

Interactive platforms have recently been developed for visualizing and annotating volumes of mega- to teravoxel size, including the Siibra-explorer and Neuroglancer. The Siibra-explorer, whose rendering capabilities build on the open-source project Neuroglancer, is a browser-based viewer of brain atlases, which allows seamless querying of semantically and spatially anchored datasets thanks to tight integration with the Human Brain Project Knowledge Graph. Currently, it contains four reference atlases and their associated images, namely the ALLEN Mouse Common Coordinate Framework [57], the Waxholm Space atlas of the Sprague Dawley rat brain [58], the Julich-Leuven Multilevel Macaque Brain [59], and the EBRAINS multilevel human brain atlas including the Julich-Brain Cytoarchitectonic Atlas [60]. The multi-resolution Neuroglancer format allows displaying tera- to petavoxel large datasets and their segmentations fast enough to be practical. It enables easy collaboration, as any view can be shared by copying the URL from the web browser. Its usefulness for collaborative brain studies has been demonstrated, for example, for segmenting the full adult fly brain dataset at 4 nm × 4 nm × 40 nm voxels, resulting in 115 TB of image data [61, 62], and lately for a connectomic microscopy study

of a 1 mm^3 volume of human cerebral cortex at 4 nm × 4 nm × 33 nm voxels, amounting to 1.4 PB of image data [63, 64]. Images in Neuroglancer format can be processed by several open software packages, including igneous [65]. In the open research platform EBRAINS, they are connected via the Siibra toolbox to various modeling and simulation cloud services for collaborative brain research [66].

8. BEING ON THE TRACK TO IMAGE THE ENTIRE HUMAN BRAIN WITH ONE MICROMETER RESOLUTION

8.1 Important milestones

More than a decade ago, our team demonstrated that bivariate histograms of registered μMRI and phase tomography data of human brain tissue permitted a direct comparison of complementary imaging techniques [67]. Recently, we extended the approach toward tri-variate histograms built from μCT-data of a distracted rat jaw before and after decalcification as well as a selected histology slide [68]. After applying k-means clustering, we could identify five tissue classes, a result which led to the hypothesis that the combination of modalities enable the discrimination of collagen types [68].

The complementarity of *post mortem* μCT and conventional histology has been demonstrated for human atherosclerotic artery segments [69] and entire mouse kidneys [70]. This analysis provided unique structural parameters on treatment-induced local shrinkage, which are essential for flow studies in vessels affected by constrictions [69] and in renal physiology [70]. Ethanol dehydration also supported the nanoscale imaging of zebrafish embryos using synchrotron radiation facilities [71]. Paraffin embedding, well established in histology, gives rise to a remarkable contrast increase in hard X-ray imaging of human brain tissue [38], which was demonstrated for isotropic spatial resolution beyond the optical limit [40] and μCT of porcine nerve using cutting-edge laboratory systems [72]. It also allowed identifying the onset of hippocampal sclerosis in a mouse model with induced temporal lobe epilepsy pathogenesis [73]. The abundance and orientation of periodic nanostructures including the myelin sheaths was quantified by means of hard X rays as well [74].

We quantitatively compared phase tomography using synchrotron radiation-based μCT (SRμCT) double-grating interferometry and conventional SRμCT in the context of paraffin-embedded human brain segments [75] and demonstrated that the contrast-to-noise ratio in phase modality was almost two times higher than the photon-energy optimized and spatial resolution-matched absorption measurements [75]. We proposed GAUSSIAN filtering of projections as alternative to PAGANIN's widespread single-distance phase retrieval filter, and proved that a GAUSSIAN filter provided a larger contrast-to-noise ratio at high spatial resolution with interpretable density measurements for brain tissue [76].

More important for the micrometer imaging of the entire brain is the detailed hard X-ray virtual histology study of the entire mouse brain over the course of standard histological preparation, *i.e.* from formalin fixation to paraffin embedding [77, 78]. By means of non-rigid registration, we quantified the embedding-dependent local microanatomy shrinkage [78]. Ethanol dehydration increased the fiber tract contrast by a factor of 15 [78]. Quantification of tissue deformations required locally adaptive transformation models with many degrees of freedom (DOFs) [78]. Further, regularization was needed to avoid overfitting and unrealistic deformations. This is of particular importance in cases, where analyzing tissue deformations is a goal of registration [78, 79]. Regularization can take the form of reduced DOFs, *e.g.* increasing spacing in the grid of control points, or adding a penalty term for large local deformations [80]. We proposed an unsupervised approach to determine the more suitable regularization approach and amount of regularization. This procedure was based on determining the image dissimilarity measures for a series of test registrations as regularization has been decreased, fitting an exponential decaying function and finding the optimum, *i.e.* closest point to [0,0] after min-max normalization [1]. This procedure was used to quantify strain fields during histological tissue preparation [57, 78].

Registration of large volumetric datasets, such as those produced from virtual histology, often leads to challenges, because the images and their spatial transformation exceed memory limits and/or cause excessive runtimes. We, therefore, developed a distributed multi-resolution approach, in the spirit of image and transformation multi-resolution pyramids, where registrations of image sub-regions are distributed to independent tasks to avoid violating memory limitations [1]. This pipeline was used to register the full-resolution mouse brain dataset to the ALLEN Mouse Brain Common Coordinate Framework [57, 81].

Automatic segmentation of anatomical regions could be challenging in label-free virtual histology, hence manual approaches were used frequently. Manual treatment, however, is infeasible for datasets of terabyte size. Improved contrast might allow for semi-automated segmentation, as validated for ethanol immersion of brain tissue to segment fiber tracts by region growing from a handful manually defined seed points in a mouse brain [82]. Machine-learning-based approaches showed success for terabyte-scale µCT of 30,000 glomeruli in a murine kidney [83]. Recently, we successfully employed a deep neural network to automatically segment the molecular, granular, and polymorph layers of the dentate gyrus on label-free µCT data with 1.6 µm-wide voxels on paraffin-embedded brain hemispheres from mice induced with temporal lobe epilepsy pathogenes [73]. We currently employ a similar segmentation strategy to automatically segment the ventricles, the choroid plexus and stroma of mouse brains from sparse slice-wise manually segmentations of sub-micron virtual histology [1]. Segmenting the single layer of choroid epithelial cells benefitted from sub-micron image resolution as well as the acquisition of the entire brain, as the choroid plexuses are present in the lateral, third and fourth ventricles.

Comprehensive brain mapping requires imaging length scales across many orders of magnitude. The human brain has a width on the order of 10 cm, the size of cells is typically on the order of micrometers, synaptic connections can be thinner than 100 nm, and morphological changes on the order of a few nanometers can affect brain circuit function. Therefore, a combination of imaging techniques is required to visualize the three-dimensional cyto-architecture of the brain. Among these, virtual histology based on µCT holds promise as a *post mortem* modality that can provide volumetric brain imaging with isotropic micrometer resolution. However, current µCT results mostly explore brain sub-volumes on the order of a few tens of cubic millimeters, while the volume of the human brain is around 1.2×10^6 mm^3. Our group has recently demonstrated imaging of an entire mouse brain with 0.65 µm-wide voxels through projection stitching, extending the imaged volume by a factor of 400 and developing a pipeline for processing these tera-voxel-sized datasets spanning the 450 mm^3 volume of the mouse brain [1, 81]. This pipeline was designed to take advantage of parallelization and run as batch jobs on either standard workstations or scientific computing infrastructure, *e.g.* with sciCORE [84] at the University of Basel, Switzerland, thus allowing for scaling to larger imaged volumes as needed for the human brain.

8.2 Preliminary results of 10 cm-wide human brain in ethanol and paraffin

In a pilot tomography study at the P07 beamline at PETRA III, Hamburg, Germany, we employed the setup, operated by the Helmholtz-Zentrum Hereon, with a monochromatic beam of 67 keV and the 80 cm sample–detector distance. We acquired radiographs with isotropic 1.27 µm-wide pixels along 1 cm-thick slices of human brain in paraffin and ethanol, cut along the coronal plane, as well as one height step acquired from an entire human brain immersed in ethanol. We extended the FOV by a factor of 20 applying projection stitching. Following the brain diameter, up to ten laterally offset scans over 360 degrees were recorded per specimen, with 48,000 partial projections each. Projections 180 degrees apart were stitched, resulting in a total of 24,000 stitched projections over 180 degrees, each 90,000 pixel wide. The ring current of the synchrotron radiation source was used for the flat-field correction.

Step and fly scan strategies were tested on centimeter-thick ethanol-dehydrated brain slices. The step scans can be combined with a random lateral movement of the specimen, which can significantly reduce the frequently observed ring artefacts in the reconstructed data, although at the cost of substantially increased scan-time overhead. For future studies, we, therefore, opt for the fly-scan acquisition strategy. Fly scans were successfully acquired for the brain slices in ethanol and paraffin as well as for the cross-sectional imaging of the entire brain. Figure 2 exemplarily shows a reconstructed slice of a 1 cm-thick brain section embedded in paraffin. The exposure time per projection was 30 ms, and eight laterally offset scans were required to span the 9.4 cm-wide FOV, resulting in a total scan time of about 3.5 hours. Figure 3 shows a selected reconstructed slice of an entire human brain immersed in 100% ethanol, imaged under identical conditions, but with ten offset scans to span 11.5 cm, resulting in about four hours scan duration.

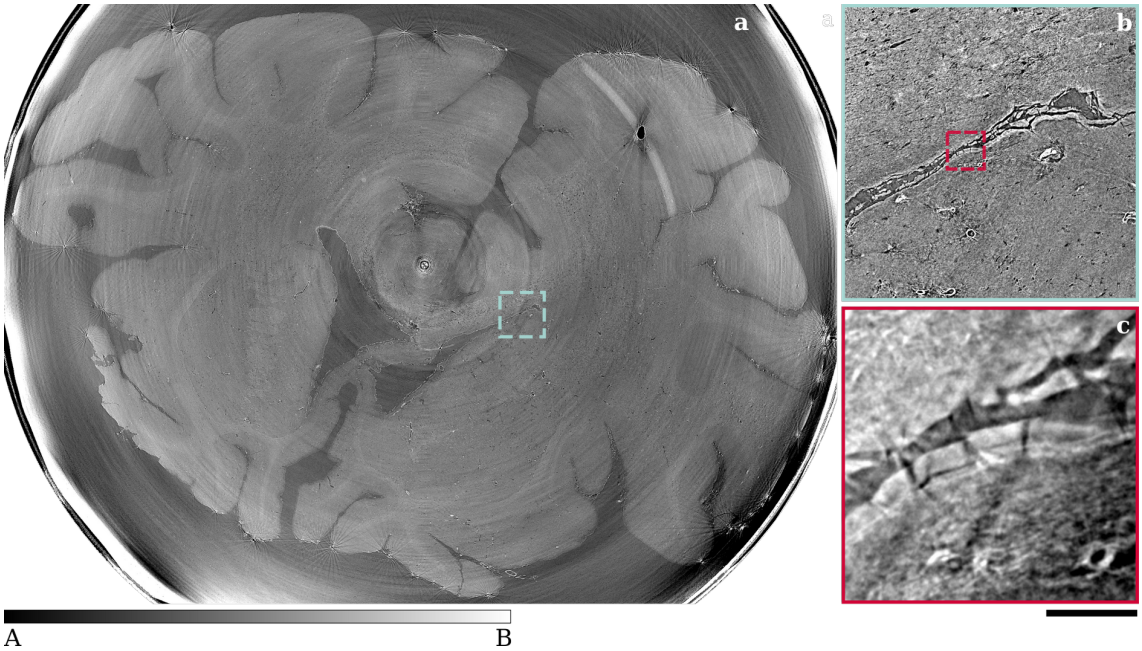

Figure 2. Virtual slice through a 1 cm-thick and more than 9 cm-wide paraffin-embedded section of the human brain. The projections were stitched from eight rings, each consisting of 48’000 images acquired over 360° with 30 ms exposure time. After 2×2 binning of the projections, the resulting isotropic voxel length was about 2.5 µm. **a** Overview over the entire section in the coronal plane. **b** and **c** Enlarged views showing the edge of a ventricle and elements of the vasculature. The intensity values span [A, B] **a** $[3.3, 4.8]\times10^{-4}$, **b** $[4.0, 6.1]\times10^{-4}$, **c** $[2.1, 4.3]\times10^{-4}$ in arbitrary units. The scale bar marks **a** 9.8 mm, **b** 1.6 mm, **c** 0.2 mm.

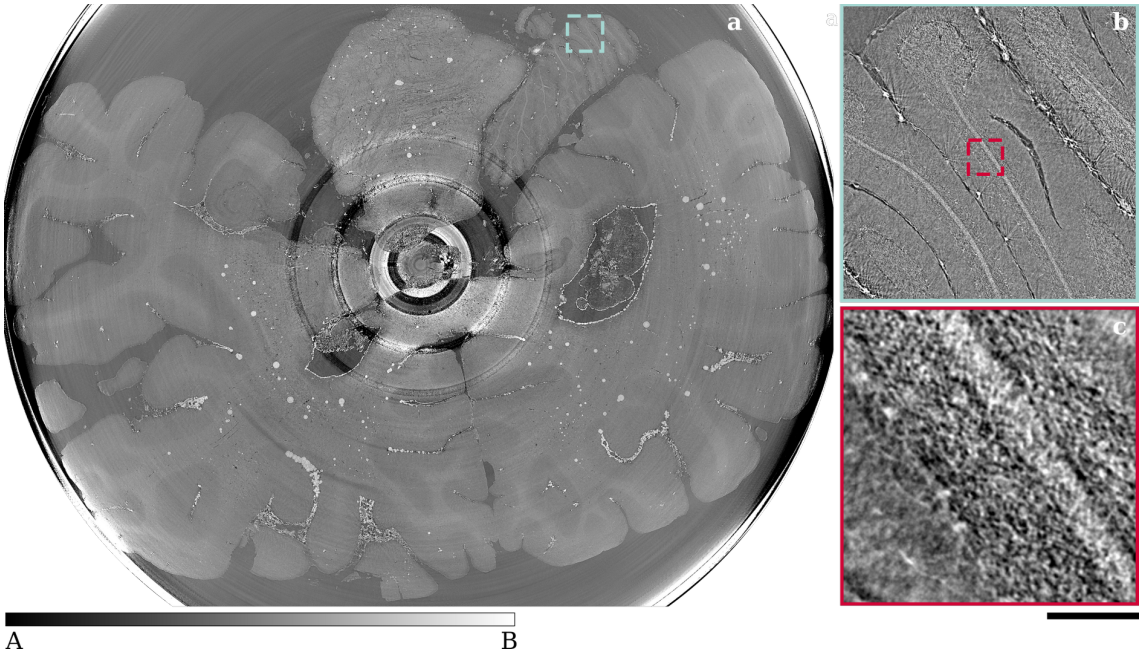

Figure 3. Virtual slice through an entire human brain immersed in 100% ethanol. The projections were stitched from ten rings, each consisting of 48’000 images acquired over 360° with 30 ms exposure time. After 2×2 binning of the projections, the resulting isotropic voxel length is 2.5 µm. **a** Overview over the entire section in the coronal plane. **b** Enlarged view showing the molecular and granular layer, white matter in the cerebellum. **c** Further enlarged view

at full spatial resolution illustrating individual Purkinje cells. The intensity values span [A, B] **a** [1.2, 4.0]×10^{-4}, **b** [1.3, 4.1]×10^{-4}, **c** [1.9, 4.9]×10^{-4} in arbitrary units. The scale bar marks **a** 12.5 mm, **b** 1.6 mm, **c** 0.2 mm.

Before reconstruction, the projection data were binned by a factor of two in order to increase the photon statistics, resulting in a total projection width of 36,940 and 45,082 pixels for the brain in paraffin and ethanol, respectively. Phase retrieval was applied to the projections [85]. Although the number of projections was substantially smaller than usually recorded for such a tomographic dataset, reasonable data quality was achieved. We could speculate that 48,000 projections would be sufficient for a 90,000 pixel-wide FOV.

9. CHALLENGES IN X-RAY IMAGING OF THE ENTIRE HUMAN BRAIN WITH ONE MICROMETER VOXEL SIZE

A human brain can be obtained from donated bodies provided that an approval of the responsible Ethical Committee is given. A professional can carefully extract the brain from the skull for formalin fixation. It takes several months to dehydrate the entire brain using an ethanol series. It is an art to embed the entire brain into paraffin. This embedding process is critical for phase tomography, because air inclusions lead to substantial artefacts.

For the SRμCT-data recording at a synchrotron radiation facility, the ethanol-immersed and paraffin-embedded brains must be suitably fixed on the rotation/translation stage. A brain-specific shape can be realized, for example, by a 3D-printed polymer container. For an efficient recording, a detector with fast data transfer capabilities is fully illuminated by a beam stable for many shifts of beamtime. The same applies to the mechanical stability of the tomography setup, which should reach sub-pixel level to avoid time-consuming post-processing.

Another challenge is the handling of big data. First, a fast accessible memory is a prerequisite. After artefact removal, normalization, and stitching, the individual slices must be reconstructed. Finally, the reconstructed data have to be registered to the related atlas with the aim to disseminate the information within the scientific community.

It is expected that the challenges can be addressed within the next four years, so that a very few datasets of the human brain will become publicly available with about 1 μm voxel size and about 2 μm spatial resolution for imaging the 10^{11} biological cells of the human brain; see https://data.snf.ch/grants/person/97306.

ACKNOWLEDGEMENT

Beamtimes 20221154 and 20230593 were granted at the beamline P07, PETRA III, DESY, Hamburg, Germany, within regular calls. The author thanks for the financial support (project 185058) from the Swiss National Science Foundation. The author gratefully acknowledges the valuable contributions of Hans Deyhle, Mattia Humbel, Griffin Rodgers, Georg Schulz, and Christine Tanner from the University of Basel, Switzerland, as well as of Felix Beckmann and Julian Moosmann from the Helmholtz-Zentrum Hereon, Germany.

REFERENCES

[1] Rodgers, G., Tanner, C., Schulz, G., Weitkamp, T., Scheel, M., Girona Alarcón, M., Kurtcuoglu, V., and Müller, B., "Mosaic microtomography of a full mouse brain with sub-micron pixel size," Proc. of SPIE **12242**, 122421L (2022).

[2] Humbel, M., Beckmann, F., Moosmann, J., Deyhle, H., Schulz, G., Tanner, C., Rodgers, G., and Müller, B., "A tomography slice through the entire human brain with less than three micrometer voxels," Proc. of SPIE **13152**, 1315220 (2024).

[3] Lichtman, J. W., and Denk, W., "The big and the small: Challenges of imaging the brain's circuits," Science **334**, 618-623 (2011).

[4] Cleary, J. O. S. H., and Guimarães, A. R., [Magnetic Resonance Imaging] Academic Press, San Diego (2014).

[5] Novikov, D. S., Fieremans, E., Jespersen, S. N., and Kiselev, V. G., "Quantifying brain microstructure with diffusion MRI: Theory and parameter estimation," NMR in Biomedicine **32**, e3998 (2019).

[6] Amunts, K., Lepage, C., Borgeat, L., Mohlberg, H., Dickscheid, T., Rousseau, M. E., Bludau, S., Bazin, P. L., Lewis, L. B., Oros-Peusquens, A. M., Shah, N. J., Lippert, T., Zilles, K., and Evans, A. C., "BigBrain: An ultrahigh-resolution 3D human brain model," Science **340**, 1472-1475 (2013).

[7] Benveniste, H., Kim, K., Zhang, L., and Johnson, G. A., "Magnetic resonance microscopy of the C57BL mouse brain," NeuroImage **11**, 601-611 (2000).

[8] Dorr, A. E., Lerch, J. P., Spring, S., Kabani, N., and Henkelman, R. M., "High resolution three-dimensional brain atlas using an average magnetic resonance image of 40 adult C57Bl/6J mice," NeuroImage **42**, 60-69 (2008).

[9] Cleary, J. O., Wiseman, F. K., Norris, F. C., Price, A. N., Choy, M., Tybulewicz, V. L. J., Ordidge, R. J., Brandner, S., Fisher, E. M. C., and Lythgoe, M. F., "Structural correlates of active-staining following magnetic resonance microscopy in the mouse brain," NeuroImage **56** 974-983 (2011).

[10] Fatterpekar, G. M., Naidich, T. P., Delman, B. N., Aguinaldo, J. G., Gultekin, S. H., Sherwood, C. C., Hof, P. R., Drayer, B. P., and Fayad, Z. A., "Cytoarchitecture of the human cerebral cortex: MR microscopy of excised specimens at 9.4 Tesla," American Journal of Neuroradiology **23**, 1313-1321 (2002).

[11] Cohen, O., and Ackerman, J. L., "Ex vivo mouse brain microscopy at 15T with loop-gap RF coil," Magnetic Resonance Imaging **51**, 1-6 (2018).

[12] Nair, G., Dodd, S., Ha, S.-K., Koretsky, A. P., and Reich, D. S., "Ex vivo MR microscopy of a human brain with multiple sclerosis: Visualizing individual cells in tissue using intrinsic iron," NeuroImage **223**, 117285 (2020).

[13] Maiter, A., Riemer, F., Allinson, K., Zaccagna, F., Crispin-Ortuzar, M., Gehrung, M., McLean, M. A., Priest, A. N., Grist, J., Matys, T., Graves, M. J., and Gallagher, F. A., "Investigating the relationship between diffusion kurtosis tensor imaging (DKTI) and histology within the normal human brain," Scientific Reports **11**, 8857 (2021).

[14] Pallast, N., Wieters, F., Fink, G. R., and Aswendt, M., "Atlas-based imaging data analysis tool for quantitative mouse brain histology (AIDAhisto)," Journal of Neuroscience Methods **326**, 108394 (2019).

[15] Schiffer, C., Harmeling, S., Amunts, K., and Dickscheid, T., "2D histology meets 3D topology: Cytoarchitectonic brain mapping with graph neural networks," Lecture Notes in Computer Science **12908** 395-404 (2021).

[16] Ding, S.-L., Royall, J. J., Sunkin, S. M., Ng, L., Facer, B. A. C., Lesnar, P., Guillozet-Bongaarts, A., McMurray, B., Szafer, A., Dolbeare, T. A., Stevens, A., Tirrell, L., Benner, T., Caldejon, S., Dalley, R. A., Dee, N., Lau, C., Nyhus, J., Reding, M., Riley, Z. L., Sandman, D., Shen, E., van der Kouwe, A., Varjabedian, A., Write, M., Zollei, L., Dang, C., Knowles, J. A., Koch, C., Phillips, J. W., Sestan, N., Wohnoutka, P., Zielke, H. R., Hohmann, J. G., Jones, A. R., Bernard, A., Hawrylycz, M. J., Hof, P. R., Fischl, B., and Lein, E. S., "Comprehensive cellular-resolution atlas of the adult human brain," Journal of Comparative Neurology **524**, 3127-3481 (2016).

[17] Aquino, D., Garbelli, R., Rossini, L., De Santis, D., Spreafico, R., d'Orio, P., Tassi, L., and Padelli, F., "A semi-automatic registration protocol to match ex-vivo high-field 7T MR images and histological slices in surgical samples from patients with drug-resistant epilepsy," Journal of Neuroscience Methods **367**, 109439 (2022).

[18] Mancini, M., Casamitjana, A., Peter, L., Robinson, E., Crampsie, S., Thomas, D. L., Holton, J. L., Jaunmuktane, Z., and Iglesias, J. E., "A multimodal computational pipeline for 3D histology of the human brain," Scientific Reports **10**, 13839 (2020).

[19] Casamitjana, A., Lorenzi, M., Ferraris, S., Peter, L., Modat, M., Stevens, A., Fischl, B., Vercauteren, T., and Iglesias, J. E., "Robust joint registration of multiple stains and MRI for multimodal 3D histology reconstruction: Application to the Allen human brain atlas," Medical Image Analysis **75**, 102265 (2022).

[20] Mizutani, R., and Suzuki, Y., "X-ray microtomography in biology," Micron **43**, 104-115 (2012).

[21] Mizutani, R., Takeuchi, A., Uesugi, K., Ohyama, M., Takekoshi, S., Osamura, R. Y., and Suzuki, Y., "Three-dimensional microtomographic imaging of human brain cortex," Brain Research **1199**, 53-61 (2008).

[22] Barbone, G. E., Bravin, A., Mittone, A., Kraiger, M. J., Hrabě de Angelis, M., Bossi, M., Ballarini, E., Rodriguez-Menendez, V., Ceresa, C., Cavaletti, G., and Coan, P., "Establishing sample-preparation protocols for X-ray phase-

contrast CT of rodent spinal cords: Aldehyde fixations and osmium impregnation," Journal of Neuroscience Methods **339**, 108744 (2020).

[23] Böhm, T., Joseph, K., Kirsch, M., Moroni, R., Hilger, A., Osenberg, M., Manke, I., Johnston, M., Stieglitz, T., Hofmann, U. G., Haas, C. A., and Thiele, S., "Quantitative synchrotron X-ray tomography of the material-tissue interface in rat cortex implanted with neural probes," Scientific Reports **9**, 7646 (2019).

[24] Anderson, R., and Maga, A. M., "A novel procedure for rapid imaging of adult mouse brains with microCT using iodine-based contrast," PLOS ONE **10**, e0142974 (2015).

[25] Saccomano, M., Albers, J., Tromba, G., Dobrivojević Radmilović, M., Gajović, S., Alves, F., and Dullin, C., "Synchrotron inline phase contrast μCT enables detailed virtual histology of embedded soft-tissue samples with and without staining," Journal of Synchrotron Radiation **25**, 1153-1161 (2018).

[26] Fonseca, M. d. C., Araujo, B. H. S., Dias, C. S. B., Archilha, N. L., Neto, D. P. A., Cavalheiro, E., Westfahl, H., da Silva, A. J. R., and Franchini, K. G., "High-resolution synchrotron-based X-ray microtomography as a tool to unveil the three-dimensional neuronal architecture of the brain," Scientific Reports **8**, 12074 (2018).

[27] Jiang, L., Li, C., Li, M., Yin, X., Wu, T., Duan, C., Cao, Y., Lu, H., and Hu, J., "Simultaneous 3D visualization of the microvascular and neural network in mouse spinal cord using synchrotron radiation micro computed tomography," Neuroscience Bulletin **37**, 1469-1480 (2021).

[28] Lareida, A., Beckmann, F., Schrott-Fischer, A., Glueckert, R., Freysinger, W., and Müller, B., "High-resolution X-ray tomography of the human inner ear: synchrotron radiation-based study of nerve fibre bundles, membranes and ganglion cells," Journal of microscopy **234**, 95-102 (2009).

[29] Momose, A., "Recent advances in X-ray phase imaging," Japanese Journal of Applied Physics **44**, 6355 (2005).

[30] Pinzer, B. R., Cacquevel, M., Modregger, P., McDonald, S. A., Bensadoun, J. C., Thuering, T., Aebischer, P., and Stampanoni, M., "Imaging brain amyloid deposition using grating-based differential phase contrast tomography," NeuroImage **61**, 1336-1346 (2012).

[31] Schulz, G., Weitkamp, T., Zanette, I., Pfeiffer, F., Beckmann, F., David, C., Rutishauser, S., Reznikova, E., and Müller, B., "High-resolution tomographic imaging of a human cerebellum: comparison of absorption and grating-based phase contrast," Journal of The Royal Society Interface **7**, 1665-1676 (2010).

[32] Barbone, G. E., Bravin, A., Romanelli, P., Mittone, A., Bucci, D., Gaaβ, T., Le Duc, G., Auweter, S., Reiser, M. F., Kraiger, M. J., Hrabě de Angelis, M., Battaglia, G., and Coan, P., "Micro-imaging of brain cancer radiation therapy using phase-contrast computed tomography," International Journal of Radiation Oncology*Biology*Physics **101**, 965-984 (2018).

[33] Zhang, M.-Q., Zhou, L., Deng, Q.-F., Xie, Y.-Y., Xiao, T.-Q., Cao, Y.-Z., Zhang, J.-W., Chen, X.-M., Yin, X.-Z., and Xiao, B., "Ultra-high-resolution 3D digitalized imaging of the cerebral angioarchitecture in rats using synchrotron radiation," Scientific Reports **5**, 14982 (2015).

[34] Dyer, E. L., Roncal, W. G., Prasad, J. A., Fernandes, H. L., Gürsoy, D., De Andrade, V., Fezzaa, K., Xiao, X., Vogelstein, J. T., Jacobsen, C., Körding, K. P., and Kasthuri, N., "Quantifying mesoscale neuroanatomy using X-ray microtomography," eNeuro **4** (5), 1-18 (2017).

[35] Hieber, S. E., Bikis, C., Khimchenko, A., Schweighauser, G., Hench, J., Chicherova, N., Schulz, G., and Müller, B., "Tomographic brain imaging with nucleolar detail and automatic cell counting," Scientific Reports **6**, 32156 (2016).

[36] Töpperwien, M., van der Meer, F., Stadelmann, C., and Salditt, T., "Three-dimensional virtual histology of human cerebellum by X-ray phase-contrast tomography," Proceedings of the National Academy of Sciences **115**, 6940-6945 (2018).

[37] Töpperwien, M., van der Meer, F., Stadelmann, C., and Salditt, T., "Correlative x-ray phase-contrast tomography and histology of human brain tissue affected by Alzheimer's disease," NeuroImage **210**, 116523 (2020).

[38] Khimchenko, A., Deyhle, H., Schulz, G., Schweighauser, G., Hench, J., Chicherova, N., Bikis, C., Hieber, S. E., and Müller, B., "Extending two-dimensional histology into the third dimension through conventional micro computed tomography," NeuroImage **139**, 26-36 (2016).

[39] Massimi, L., Bukreeva, I., Santamaria, G., Fratini, M., Corbelli, A., Brun, F., Fumagalli, S., Maugeri, L., Pacureanu, A., Cloetens, P., Pieroni, N., Fiordaliso, F., Forloni, G., Uccelli, A., Kerlero de Rosbo, N., Balducci, C., and Cedola, A., "Exploring Alzheimer's disease mouse brain through X-ray phase contrast tomography: From the cell to the organ," NeuroImage **184**, 490-495 (2019).

[40] Khimchenko, A., Bikis, C., Pacureanu, A., Hieber, S. E., Thalmann, P., Deyhle, H., Schweighauser, G., Hench, J., Frank, S., Müller-Gerbl, M., Schulz, G., Cloetens, P., and Müller, B., "Hard X-ray nanoholotomography: Large-scale, label-free, 3D neuroimaging beyond optical limit," Advanced Science **5**, 1700694 (2018).

[41] Kuan, A. T., Phelps, J. S., Thomas, L. A., Nguyen, T. M., Han, J., Chen, C.-L., Azevedo, A. W., Tuthill, J. C., Funke, J., Cloetens, P., Pacureanu, A., and Lee, W.-C. A., "Dense neuronal reconstruction through X-ray holographic nano-tomography," Nature Neuroscience **23**, 1637-1643 (2020).

[42] Albers, J., Pacilé, S., Markus, M. A., Wiart, M., Vande Velde, G., Tromba, G., and Dullin, C., "X-ray-based 3D virtual histology—adding the next dimension to histological analysis," Molecular Imaging and Biology **20**(5), 732-741 (2018).

[43] Katsamenis, O. L., Olding, M., Warner, J. A., Chatelet, D. S., Jones, M. G., Sgalla, G., Smit, B., Larkin, O. J., Haig, I., Richeldi, L., Sinclair, I., Lackie, P. M., and Schneider, P., "X-ray micro computed tomography for nondestructive three-dimensional X-ray histology," The American Journal of Pathology **189**, 1608-1620 (2019).

[44] Uludağ, K., and Roebroeck, A., "General overview on the merits of multimodal neuroimaging data fusion," NeuroImage **102**, 3-10 (2014).

[45] Du, M., Vescovi, R., Fezzaa, K., Jacobsen, C., and Gürsoy, D., "X-ray tomography of extended objects: A comparison of data acquisition approaches," Journal of the Optical Society of America A **35**, 1871-1879 (2018).

[46] Kyrieleis, A., Ibison, M., Titarenko, V., and Withers, P. J., "Image stitching strategies for tomographic imaging of large objects at high resolution at synchrotron sources," Nuclear Instruments and Methods in Physics Research Section A: Accelerators, Spectrometers, Detectors and Associated Equipment **607**, 677-684 (2009).

[47] Vescovi, R., Du, M., de Andrade, V., Scullin, W., Gürsoy, D., and Jacobsen, C., "Tomosaic: efficient acquisition and reconstruction of teravoxel tomography data using limited-size synchrotron X-ray beams," Journal of Synchrotron Radiation **25**, 1478-1489 (2018).

[48] Vo, N. T., Atwood, R. C., Drakopoulos, M., and Connolley, T., "Data processing methods and data acquisition for samples larger than the field of view in parallel-beam tomography," Optics Express **29**, 17849-17874 (2021).

[49] Kyrieleis, A., Titarenko, V., Ibison, M., Connolley, T., and Withers, P. J., "Region-of-interest tomography using filtered backprojection: Assessing the practical limits," Journal of microscopy **241**, 69-82 (2011).

[50] Robisch, A. L., Frohn, J., and Salditt, T., "Iterative micro-tomography of biopsy samples from truncated projections with quantitative gray values," Physics in Medicine & Biology **65**, 235034 (2020).

[51] da Silva, J. C., Guizar-Sicairos, M., Holler, M., Diaz, A., van Bokhoven, J. A., Bunk, O., and Menzel, A., "Quantitative region-of-interest tomography using variable field of view," Optics Express **26**, 16752-16768 (2018).

[52] Borisova, E., Lovric, G., Miettinen, A., Fardin, L., Bayat, S., Larsson, A., Stampanoni, M., Schittny, J. C., and Schlepütz, C. M., "Micrometer-resolution X-ray tomographic full-volume reconstruction of an intact post-mortem juvenile rat lung," Histochemistry and Cell Biology **155**, 215-226 (2021).

[53] Miettinen, A., Oikonomidis, I. V., Bonnin, A., and Stampanoni, M., "NRStitcher: non-rigid stitching of terapixel-scale volumetric images," Bioinformatics **35**, 5290-5297 (2019).

[54] Trinkle, S., Foxley, S., Kasthuri, N., and Rivière, P. L., "Synchrotron X-ray micro-CT as a validation dataset for diffusion MRI in whole mouse brain," Magnetic Resonance in Medicine **86**, 1067-1076 (2021).

[55] Foxley, S., Sampathkumar, V., De Andrade, V., Trinkle, S., Sorokina, A., Norwood, K., La Riviere, P., and Kasthuri, N., "Multi-modal imaging of a single mouse brain over five orders of magnitude of resolution," NeuroImage **238**, 118250 (2021).

[56] Walsh, C. L., Tafforeau, P., Wagner, W. L., Jafree, D. J., Bellier, A., Werlein, C., Kühnel, M. P., Boller, E., Walker-Samuel, S., Robertus, J. L., Long, D. A., Jacob, J., Marussi, S., Brown, E., Holroyd, N., Jonigk, D. D.,

Ackermann, M., and Lee, P. D., "Imaging intact human organs with local resolution of cellular structures using hierarchical phase-contrast tomography," Nature Methods **18**, 1532-1541 (2021).

[57] Wang, Q., Ding, S.-L., Li, Y., Royall, J., Feng, D., Lesnar, P., Graddis, N., Naeemi, M., Facer, B., Ho, A., Dolbeare, T., Blanchard, B., Dee, N., Wakeman, W., Hirokawa, K. E., Szafer, A., Sunkin, S. M., Oh, S. W., Bernard, A., Phillips, J. W., Hawrylycz, M., Koch, C., Zeng, H., Harris, J. A., and Ng, L., "The Allen mouse brain common coordinate framework: A 3D reference atlas," Cell **181**, 936-953.e20 (2020).

[58] Papp, E. A., Leergaard, T. B., Calabrese, E., Johnson, G. A., and Bjaalie, J. G., "Waxholm Space atlas of the Sprague Dawley rat brain," NeuroImage **97**, 374-386 (2014).

[59] Rapan, L., Froudist-Walsh, S., Niu, M., Xu, T., Funck, T., Zilles, K., and Palomero-Gallagher, N., "Multimodal 3D atlas of the macaque monkey motor and premotor cortex," NeuroImage **226**, 117574 (2021).

[60] Amunts, K., Mohlberg, H., Bludau, S., and Zilles, K., "Julich-Brain: A 3D probabilistic atlas of the human brain's cytoarchitecture," Science **369**(6506), 988-992 (2020).

[61] Zheng, Z., Lauritzen, J. S., Perlman, E., Robinson, C. G., Nichols, M., Milkie, D., Torrens, O., Price, J., Fisher, C. B., and Sharifi, N., "A complete electron microscopy volume of the brain of adult Drosophila melanogaster," Cell **174**, 730-743 (2018).

[62] [FAFB-FFN1 Full Adult Fly Brain Automated Segmentation on Neuroglancer].

[63] [H01 dataset, a small sample of human brain tissue and its segmentations with Neuroglancer].

[64] Shapson-Coe, A., Januszewski, M., Berger, D. R., Pope, A., Wu, Y., Blakely, T., Schalek, R. L., Li, P. H., Wang, S., and Maitin-Shepard, J., "A connectomic study of a petascale fragment of human cerebral cortex," BioRxiv, (2021).

[65] Silversmith, W., Zlateski, A., Bae, J. A., Tartavull, I., Kemnitz, N., Wu, J., and Seung, H. S., "Igneous: Distributed dense 3D segmentation meshing, neuron skeletonization, and hierarchical downsampling," Frontiers in Neural Circuits **16**, 977700 (2022).

[66] Schirner, M., Domide, L., Perdikis, D., Triebkorn, P., Stefanovski, L., Pai, R., Prodan, P., Valean, B., Palmer, J., and Langford, C., "Brain simulation as a cloud service: The virtual brain on EBRAINS," NeuroImage **251**, 118973 (2022).

[67] Schulz, G., Waschkies, C., Pfeiffer, F., Zanette, I., Weitkamp, T., David, C., and Müller, B., "Multimodal imaging of human cerebellum - merging X-ray phase microtomography, magnetic resonance microscopy and histology," Scientific Reports **2**, 826 (2012).

[68] Rodgers, G., Sigron, G., Tanner, C., Hieber, S. E., Beckmann, F., Schulz, G., Scherberich, A., Jaquiéry, C., Christoph, K., and Müller, B., "Combining high-resolution hard X-ray tomography and histology for stem cell-mediated distraction osteogenesis," Applied Sciences **12**, 6286 (2022).

[69] Buscema, M., Hieber, S. E., Schulz, G., Deyhle, H., Hipp, A., Beckmann, F., Lobrinus, J. A., Saxer, T., and Müller, B., "Ex vivo evaluation of an atherosclerotic human coronary artery via histology and high-resolution hard X-ray tomography," Scientific Reports **9**, 14348 (2019).

[70] Kuo, W., Le, N. A., Spingler, B., Wenger, R. H., Kipar, A., Hetzel, U., Schulz, G., Müller, B., and Kurtcuoglu, V., "Simultaneous three-dimensional vascular and tubular imaging of whole mouse kidneys with X-ray μCT," Microscopy and Microanalysis **26**, 731-740 (2020).

[71] Cörek, E., Rodgers, G., Siegrist, S., Einfalt, T., Detampel, P., Schlepütz, C. M., Sieber, S., Fluder, P., Schulz, G., Unterweger, H., Alexiou, C., Müller, B., Puchkov, M., and Huwyler, J., "Shedding light on metal-based nanoparticles in zebrafish by computed tomography with micrometer resolution," Small **16**, 2000746 (2020).

[72] Migga, A., Schulz, G., Rodgers, G., Osterwalder, M., Tanner, C., Blank, H., Jerjen, I., Salmon, P., Twengström, W., Scheel, M., Weitkamp, T., Schlepütz, C. M., Bolten, J. S., Huwyler, J., Hotz, G., Madduri, S., and Müller, B., "Comparative hard x-ray tomography for virtual histology of zebrafish larva, human tooth cementum, and porcine nerve," Journal of Medical Imaging **9**, 031507 (2022).

[73] Rodgers, G., Bikis, C., Janz, P., Tanner, C., Schulz, G., Thalmann, P., Haas, C. A., and Müller, B., "3D X-ray histology for the investigation of temporal lobe epilepsy in a mouse model," Microscopy and Microanalysis **29**, 1730-1745 (2023).

[74] Schulz, G., Deyhle, H., Bikis, C., Bunk, O., and Müller, B., "Imaging the orientation of myelin sheaths in a non-stained histology slide of human brain," Precision Nanomedicine **3**, 656–665 (2020).

[75] Bikis, C., Rodgers, G., Deyhle, H., Thalmann, P., Hipp, A., Beckmann, F., Weitkamp, T., Theocharis, S., Rau, C., Schulz, G., and Müller, B., "Sensitivity comparison of absorption and grating-based phase tomography of paraffin-embedded human brain tissue," Applied Physics Letters **114**, 083702 (2019).

[76] Rodgers, G., Schulz, G., Deyhle, H., Kuo, W., Rau, C., Weitkamp, T., and Müller, B., "Optimizing contrast and spatial resolution in hard X-ray tomography of medically relevant tissues," Applied Physics Letters **116**, 023702 (2020).

[77] Rodgers, G., Kuo, W., Schulz, G., Scheel, M., Migga, A., Bikis, C., Tanner, C., Kurtcuoglu, V., Weitkamp, T., and Müller, B., "Virtual histology of an entire mouse brain from formalin fixation to paraffin embedding. Part 1: Data acquisition, anatomical feature segmentation, tracking global volume and density changes," Journal of Neuroscience Methods **364**, 109354 (2021).

[78] Rodgers, G., Tanner, C., Schulz, G., Migga, A., Kuo, W., Bikis, C., Scheel, M., Kurtcuoglu, V., Weitkamp, T., and Müller, B., "Virtual histology of an entire mouse brain from formalin fixation to paraffin embedding. Part 2: Volumetric strain fields and local contrast changes," Journal of Neuroscience Methods **365**, 109385 (2022).

[79] Schulz, G., Crooijmans, H. J. A., Germann, M., Scheffler, K., Müller-Gerbl, M., and Müller, B., "Three-dimensional strain fields in human brain resulting from formalin fixation," Journal of Neuroscience Methods **202**, 17-27 (2011).

[80] Rodgers, G., Schulz, G., Kuo, W., Scheel, M., Kurtcuoglu, V., Weitkamp, T., Müller, B., and Tanner, C., "Non-rigid registration to determine strain fields during mouse brain fixation and embedding," Proc. of SPIE **11586**, 115860I (2021).

[81] Humbel, M., Tanner, C., Schulz, G., Weitkamp, T., Scheel, M., Girona Alarcón, M., Kurtcuoglu, V., Müller, B., and Rodgers, G., [Mosaic microtomography of an entire mouse brain with sub-micron pixel size] EBRAINS, (2023).

[82] Rodgers, G., Tanner, C., Schulz, G., Migga, A., Weitkamp, T., Kuo, W., Scheel, M., Osterwalder, M., Kurtcuoglu, V., and Müller, B., "Impact of fixation and paraffin embedding on mouse brain morphology: A synchrotron radiation-based tomography study," Proc. of SPIE **11840**, 118400P (2021).

[83] Kuo, W., Rossinelli, D., Schulz, G., Wenger, R. H., Hieber, S., Müller, B., and Kurtcuoglu, V., "Terabyte-scale supervised 3D training and benchmarking dataset of the mouse kidney," Scientific Data **10**, 510 (2023).

[84] sciCORE, [http://scicore.unibas.ch/].

[85] Moosmann, J., Ershov, A., Weinhardt, V., Baumbach, T., Prasad, M. S., LaBonne, C., Xiao, X., Kashef, J., and Hofmann, R., "Time-lapse X-ray phase-contrast microtomography for in vivo imaging and analysis of morphogenesis," Nature Protocols **9**, 294-304 (2014).